Scientific paper

The Preparation and Thermal Behavior of Calcium Monocarboaluminate

Roman Gabrovšek,[a] Tomaž Vuk[b] and Venčeslav Kaučič[a]

[a]National Institute of Chemistry, P. O. Box 660, SI-1001 Ljubljana, Slovenia

[b]Salonit Anhovo, Building Materials, Joint-Stock Co., SI-5210 Deskle, Slovenia

* Corresponding author: E-mail: roman.gabrovsek@ki.si

Received: 18-04-2008

Dedicated to the memory of Professor Ljubo Golič

Abstract

The synthesis of calcium monocarboaluminate starting from mixtures comprising gibbsite or boehmite, portlandite and limestone was carried out at 80 °C with synthesis times of 24 and 48 hours. Products were characterized by powder X-ray diffraction, thermogravimetric analysis, IR spectroscopy and scanning electron microscopy. Products differed in calcium monocarboaluminate content, unreacted portlandite and limestone contents also varied. The differences in X-ray diffraction patterns and IR spectra were less pronounced. Scanning electron micrographs showed two different sizes of calcium monocarboaluminate hexagonal platy crystals. Thermogravimetric curves revealed three or four dehydration steps of calcium monocarboaluminate indicating different water contents, depending on starting materials combination and, to a lesser extent, on synthesis conditions. The main effect on the formation of calcium monocarboaluminate from the above starting materials was a combination of aluminum source and limestone particle size.

Keywords: Calcium monocarboaluminate; synthesis; X-ray diffraction; thermogravimetric analysis; activation energy

1. Introduction

Calcium monocarboaluminate, more accurately designated as tetra calcium monocarboaluminate 11-hydrate, $3CaO.Al_2O_3.CaCO_3.11H_2O$ ($C_4A\bar{C}H_{11}$ in cement chemistry notation; C = CaO, A = Al_2O_3, $\bar{C}$ = CO_2, H = H_2O) has been frequently referred to in the scientific cement-related literature as either monocarbonate (used hereafter) or carboaluminate. It represents an AFm-type hydrated phase that easily forms as a product of a reaction between various calcium aluminate hydrates and atmospheric CO_2 and its presence is also a consequence of the exposure of calcium aluminate cements to the air.[1, 2]

Our interest in monocarbonate stems from our ongoing research on effects of the use of limestone, having different particle size distributions, as an admixture during portland cement hydration and monocarbonate formation during this process and in monocarbonate presence as the consequence of an interfacial zone reaction between hydrating cement paste and calcareous aggregate.[3–9] Various aspects and conditions for the formation of monocarbonate during the hydration of limestone-containing portland cement pastes have been extensively documented through studies conducted particularly over the last 20 years.[10–16]

The assessment and characterization of monocarbonate presence had been generally performed for a number of decades and usually dealt with research-specific topics.[17–24]

Literature data on syntheses of more or less pure monocarbonate are rare but there is evidence that syntheses almost invariably started from various calcium- or sodium aluminates in the presence of various sources of carbonate ions.[25] The mechanism of monocarbonate formation was described as a multi step process: at first there was a reaction between hydrated calcium cations and aluminate anions resulting in the appearance of hydrated calcium hydroxoaluminate exhibiting a disordered layered structure with a basal spacing of 1.08 nm or more; the next step was an ion substitution, facilitated by a large interlayer distance, of $2OH^-$ by $1CO_3^{2-}$, and finally a reordering of a layer structure accompanied by the basal spacing shrinkage to a final characteristic value of 0.76 nm was accomplished.[26] The author, however, did not offer any

experimental evidence to support his proposed mechanism. Monocarbonate presence was most frequently confirmed by X-ray diffraction[27–31] and infrared spectroscopy (IR).[32–36]

The crystal structure of $C_4A\bar{C}H_{11}$ was determined from a single crystal originating from an old concrete block[37] and also from a synthetic single crystal prepared hydrothermally under high pressure.[38,39] The lamellar structure contained only one type of structural element, $[Ca_2Al(OH)_6]^+$, as the main layer, and $[½CO_3{\cdot}2.5H_2O]^-$ as the interlayer element. The interlayer space was occupied by carbonate anions and three out of five randomly distributed water molecules.

The purpose of our research was the synthesis of monocarbonate by using different alumina- and limestone sources, its characterization and the assessment of its thermal behavior. Thermal dehydration of monocarbonate-containing products was evaluated by thermogravimetric analysis that has been an established and reliable method for diverse applications in studies of hydrated cements and related compounds.[40–44] We wanted to evaluate and ascertain any existing interrelation(s) between alumina source and calcite particle size distribution with regard to monocarbonate formation.

2. Experimental

Boehmite, AlO(OH), Pural SB-1 (Sasol Germany GmbH); gibbsite, $Al(OH)_3$ (Merck KGaA); portlandite, $Ca(OH)_2$ (Sigma-Aldrich) and two natural, ground limestones, Magnesia 448 (Magnesia GmbH, Germany), calcite 4.2 hereafter and Calplex Extra (Calcit d.o.o., Slovenia); calcite 0.8 hereafter, were used as starting materials. Their characteristics are given in Table 1.

Table 1. Physico-chemical properties of the starting materials.

Material	Purity	Surface area BET–N_2 (m^2/g)	D_{50} (μm)
Boehmite	77.9% Al_2O_3	290	–
Gibbsite	64.6% Al_2O_3	0.33	–
Portlandite	95+% $Ca(OH)_2$	–	–
Magnesia 448	99.6% $CaCO_3$	2.1	4.2
Calplex Extra	98.1% $CaCO_3$	9.7	0.83

2. 1. The Synthesis

Mixtures with molar ratios corresponding to theoretical values were prepared and homogenized. Powders were transferred into polyethylene vials and prewarmed to the specific synthesis temperature. Deionized water with the same temperature was then added (w/s ratio of 1). Pastes were additionally sonicated with VibraCell ultrasonic probe (Sonics & Materials Inc., Danbury, U.S.A.) for 30 seconds, flushed with pure nitrogen so as to minimize the effect of atmospheric CO_2 and vials were capped airtight. Preliminary runs were performed at 70, 80 and 90 °C for 24- and 48 hours. Products from 70-degree runs had large contents of unreacted portlandite and limestone, whereas products obtained at 90 °C contained significant quantities of hydrogarnet, C_3AH_6. The synthesis temperature of 80 °C was therefore chosen as an acceptable choice and only the products obtained at this temperature were used. After the completion of syntheses products were filtered and residual water removed by using isopropanol and diethyl ether. Products were dried overnight at 35 °C in a forced-air oven and kept in a desiccator.

2. 2. Instrumental Characterization

Powder X-ray diffraction was carried out with a high-resolution PANalytical X'PERT PRO instrument with Cu Kα1 radiation. Measurement range was from 10 to 50 2ϑ with 0.034 steps integrated at the rate of 100 s per step when using standard rotating sample holder step.

Thermal analyses were run on a SDT 2960 Simultaneous DSC-TGA instrument (TA Instruments–Waters LLC, USA) at 10 /min from 25 to 915 °C in 100 mL/min N_2 flow. Prior to the analysis each sample was held isothermally at 25 °C for 30 minutes in the flow of N_2 in the instrument. All results were determined from DTG curves with integration limits determined by the inspection of the second derivative pattern of each DTG curve. Results were recalculated with regard to the ignited mass at 915 °C for each sample investigated. This procedure facilitates comparisons among samples with similar compositions but having different mass losses at the end of a run.

Infrared spectra were recorded on a Perkin-Elmer 2000 FTIR spectrometer using KBr pellet technique in absorbance mode from 400 to 4000 cm^{-1} with a resolution of 2 cm^{-1}.

Morphology of products was examined by using a Carl Zeiss Supra 35VP scanning electron microscope (SEM). Observations were performed in BSE mode on uncoated samples.

3. Results

3. 1. Powder X-ray Diffraction

The presence of monocarbonate in products was assessed by the search-match comparison of experimental X-ray diffraction pattern to ICDD PDF 2 Ref. Code 01-087-0493 data by using X'Pert High Score Plus software. There were 42 reflections found ($I/I_o \geq 1$). Reflections of hydrogarnet (katoite), C_3AH_6 (ICDD PDF 2 Ref. Code 01-072-1109), were present in all but two products, and traces of calcite, $C\bar{C}$ (ICDD PDF 2 Ref Code 01-085-1108), were present in some samples. No other phases were identified in products. Figure 1 shows the X-ray diffraction pattern of a synthetic monocarbonate. The intensity scale

has been limited to show enhanced details of the scan. Two of the most intense reflections of monocarbonate I_{100} (11.669 2θ, d = 0.7577 nm) and I_{90} (23.481 2θ, d = 0.3786 nm) with 20,662 and 11,906 counts, respectively, are for this particular sample thus off scale.

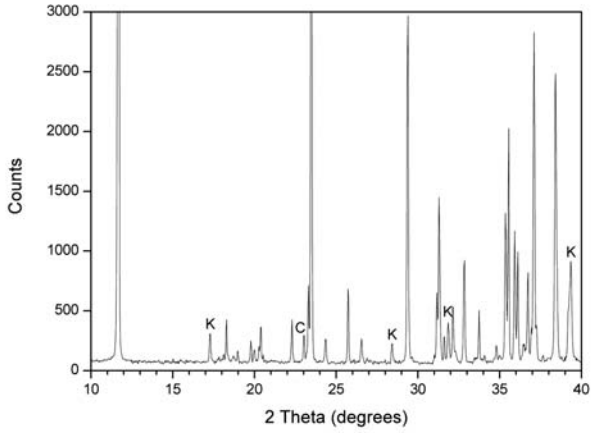

Figure 1. Powder X-ray diffraction pattern of a synthetic boehmite+calcite 4.2-based monocarbonate (48 h). All reflections from monocarbonate, except K: katoite (C_3AH_6) and C: calcite.

Semi quantitative monocarbonate and hydrogarnet contents in products (Table 2) were calculated by X'Pert High Score Plus software on the basis of Reference Intensity Ratios (RIR) given in the corresponding ICDD PDF 2 data cards.

The values in Table 2 should be regarded primarily as indicators of monocarbonate contents that are a consequence of using different combination of starting materials and synthesis times at 80 °C. When finer limestone was used, calcite 0.8, the alumina source shows greater influence on monocarbonate formation that the synthesis time does. The opposite clearly holds for the syntheses where coarser limestone, calcite 4.2, was used.

Cell parameters were determined by the use of UnitCell program[45]; hkl indices were taken from published data.[37] Table 3 shows crystallographic data for a synthetic monocarbonate; for the comparison also crystallographic data for a single crystal, formed in a 2-year old concrete block, are listed.[37]

Table 3. Calculated cell parameters of a synthetic monocarbonate.

Parameter	This work*	(Ref.37)
a_o (nm)	0.57790.0005	0.57810.0001
b_o (nm)	0.57390.0006	0.57440.0001
c_o (nm)	0.78440.0005	0.78550.0001
α ()	92.630.03	92.610.02
β ()	101.960.02	101.960.02
γ ()	120.070.02	120.090.02
V (nm^3)	0.21740.0001	0.2173 ± (not given)

* Uncertainties are given as 95% confidence interval.

3. 2. Thermal Analysis

Thermogravimetric curves of monocarbonate prepared by using gibbsite as an alumina source exhibit several mass losses from 120 to 915 °C. A characteristic TG-DTG curve is shown in Figure 2.

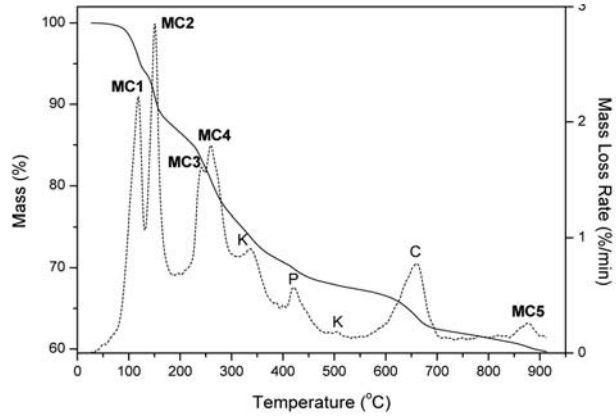

Figure 2. TG-DTG curve of a gibbsite+calcite 4.2-based monocarbonate.MC1-MC5: monocarbonate; K: katoite; P: portlandite; C: calcite.

Table 2. Semi quantitative compositions of synthetic monocarbonate products.

Content (%)		Synthesis conditions		
Monocarbonate	Hydrogarnet	Alumina source	Calcite source	Synthesis time (hours)
100	0	AlOOH	Calcite 0.8	48
100	0	AlOOH	Calcite 0.8	24
98	2	$Al(OH)_3$	Calcite 0.8	48
96	4	$Al(OH)_3$	Calcite 0.8	24
95	5	AlOOH	Calcite 4.2	48
95	5	$Al(OH)_3$	Calcite 4.2	48
93	7	AlOOH	Calcite 4.2	24
92	8	$Al(OH)_3$	Calcite 4.2	24

The first four mass loses from 120 to 285 °C, represented by two doublets, show dehydration steps of a monocarbonate (MC1-MC4 in Fig. 2). The next mass loss (K in Fig. 2) at about 335 °C represents the first step of the dehy-

dration of hydrogarnet. Thermal decomposition of portlandite at about 430 °C (P in Fig. 2) follows next. The second dehydration step of hydrogarnet takes place at about 515 °C (K in Fig. 2).[46] The next mass loss at about 670 °C indicates the thermal decomposition of limestone (C in Fig. 2) and the final mass loss near 865 °C (MC5 in Fig. 2) represents the decarboxylation of a monocarbonate.[47]

A characteristic thermogravimetric curve of a monocarbonate prepared from boehmite as an alumina source is shown in Fig. 3; it differs from the gibbsite-based one in several features: it shows only the first doublet of monocarbonate dehydration (MC1 and MC2 in Fig. 3); the second doublet has merged into one broad asymmetric peak (MC3 in Fig. 3). The two steps of hydrogarnet dehydration are missing. The dehydration of portlandite (P in Fig. 3) exhibits a two-step process. The decomposition of unreacted limestone (C in Fig.3) and the decarboxylation of monocarbonate (MC4 in Fig. 3) are also evident.

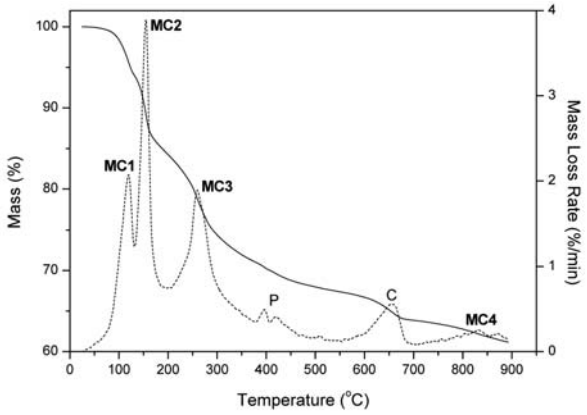

Figure 3. TG-DTG curve of a boehmite+calcite 4.2-based monocarbonate.MC1-MC4, monocarbonate; P, portlandite; C, calcite.

3. 2. 1. Gibbsite-based Monocarbonate

Gibbsite-based products showed only minor influence of calcite source and synthesis time on either temperatures of DTG maxima or shapes of DTG curves as shown in Figures 4 and 5.

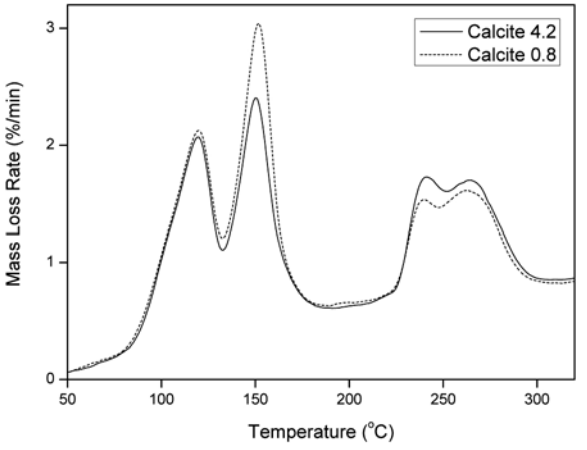

Figure 4. The influence of calcite source on the shape of DTG curves (24-h synthesis).

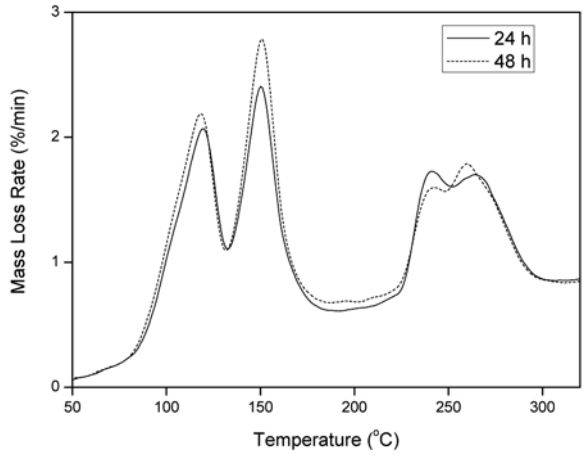

Figure 5. The influence of synthesis time on the shape of DTG curves (Calcite 4.2 used).

Characteristic dehydration temperatures of DTG maxima of gibbsite-based monocarbonates are as follows: 120±1 °C (MC1), 151±1 °C (MC2), 241±1 °C (MC3) and 262±1 °C (MC4).

Experimental mass losses of individual dehydration steps were calculated as moles of water. The results are shown in Table 4.

Water contents of MC1 and MC2 show a small decreasing trend with longer synthesis time regardless of the calcite fraction used whereas water contents of MC3 show the opposite trend. Water contents of MC4 show an unexpected behavior seemingly depending on the calcite fraction used.

Monocarbonate samples were isothermally heated at 110, 120 and 130 °C (approx. ±10 °C of MC1 temperature) for 2 hours in order to establish the thermal stability of four dehydration steps. The results are shown in Figure 6.

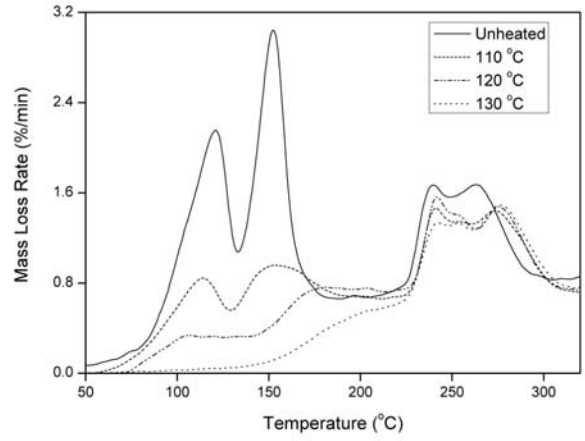

Figure 6. Dehydration behavior of gibbsite-based monocarbonate after heating at indicated temperatures.

Table 4. Water content of individual dehydration steps of gibbsite-based monocarbonates.

Water content (moles)				Synthesis conditions	
MC1	MC2	MC3	MC4	Limestone source	Synthesis time (hours)
1.80	2.27	1.40	1.84	Calcite 0.8	24
1.78	2.18	1.57	1.87	Calcite 0.8	48
1.80	2.19	1.50	1.94	Calcite 4.2	24
1.73	1.99	1.60	1.90	Calcite 4.2	48

The area under MC1 and MC2 peaks significantly decreased after heating at 110 °C, decreased even more after heating at 120 °C and became a shoulder on the lower-temperature side of MC3 and MC4 doublet after heating at 130 °C. Powder X-ray diffraction of heated samples showed markedly decreased intensities of monocarbonate reflections, however, no distinct changes in cell parameters were observed.

The contents of unreacted portlandite and limestone in products were low, on the average 2.5% for the former and 3.6% for the latter.

Apparent activation energies of four dehydration steps were determined from DTG curves by Kissinger method.[48] This method uses the correlation between peak temperature, T_p (K), and heating rate, β (/min), for several different heating rates in the form: $d(\ln \beta/T^2_p)/d(1/T_p) = -E/R$. From the slope of a linear plot of log (β/T^2_p) vs T^{-1}_p, based on experimental DTG data, an apparent activation energy can be calculated by the equation, E_a = Slope x R x 2.303, where E_a is the apparent activation energy (kJ/mole) and R is the gas constant (8.314 J mol^{-1} K^{-1}). Samples (5–6 mg) were heated at 1.5, 3, 6 and 12 /min; all plots were linear with correlation coefficients, $r \geq 0.9960$. Standard deviations of fits as well as standard errors of regression coefficients were low and all regressions were highly significant with $p < 0.01$. Calculated activation energies (rounded to the nearest whole number) for dehydration steps are listed in Table 5.

Table 5. Apparent activation energies for dehydration steps of gibbsite-based monocarbonates.

Dehydration step	E_a (kJ/mole)	± (kJ/mole)
MC1	85	1
MC2	105	7
MC3	454	24
MC4	184	9

3. 2. 2. Boehmite-based Monocarbonate

Boehmite-based products also exhibited only minor influence of calcite source and synthesis time on both temperatures of DTG maxima and shapes of DTG curves. The effects are shown in Figures 7 and 8.

Characteristic dehydration temperatures of DTG maxima of boehmite-based monocarbonates are as follows: 121±1 °C (MC1), 155±1 °C (MC2) and 261±1 °C

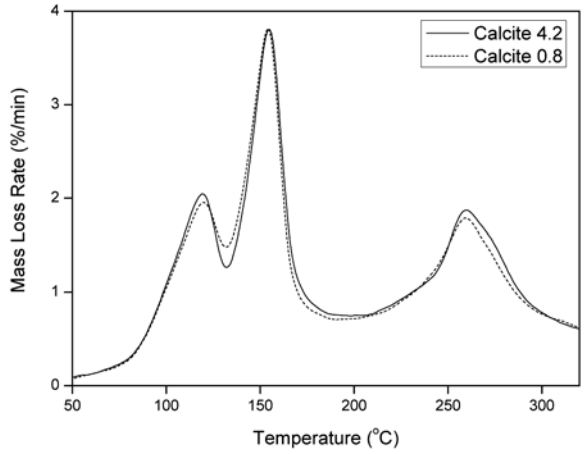

Figure 7: The influence of calcite source on the shape of DTG curves of boehmite-based monocarbonates (24-h synthesis).

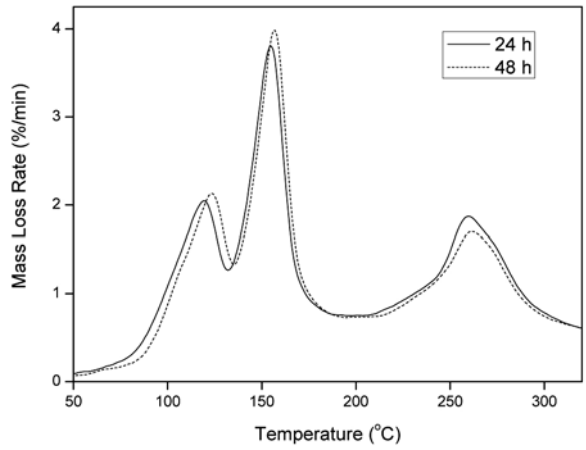

Figure 8. The influence of synthesis time on the shape of DTG curves of boehmite-based monocarbonates (Calcite 4.2 used).

(MC3). The decomposition of portlandite for boehmite-based monocarbonates was invariably a two-step process with maxima at 395±1 and 422±2 °C. The first step most likely represents an effect of the dehydration of C_3AH_6 that transformed into $C_{12}A_7H$ and CH.[49] The DTG peak area of this step increased considerably when calcite 4.2 was used when compared with a corresponding area in products where calcite 0.8 was used. The DTG peak area of the second dehydration step, indicating the dehydroxylation of unreacted port-

landite, showed no dependency on the limestone fraction used.

Experimental mass losses from the dehydration of monocarbonate (MC1-MC3) were calculated as moles of water released and they are shown in Table 6

Table 6. Water content of individual dehydration steps of boehmite-based monocarbonates.

Water content (moles)			Synthesis conditions	
MC1	MC2	MC3	Limestone source	Synthesis time (hours)
1.75	2.98	2.98	Calcite 0.8	24
1.79	3.00	2.95	Calcite 0.8	48
1.78	3.07	3.11	Calcite 4.2	24
1.76	2.93	3.16	Calcite 4.2	48

The water content of individual steps of boehmite-based monocarbonates is rather insensitive to either limestone source used or synthesis time. There is only a noticeable increase in water content in MC3 step when coarser fraction of limestone, calcite 4.2, was used.

Products of boehmite-based monocarbonates showed after heating at 110, 120 and 130 °C the behavior similar to gibbsite-based products mentioned above.

The contents of unreacted portlandite and limestone within these products were also low. The average contents of remaining portlandite and limestone were 1.8% and 2.2%, respectively.

Table 7. Apparent activation energies for dehydration steps of boehmite-based monocarbonates.

Dehydration step	Ea (kJ/mole)	± (kJ/mole)
MC1	85	9
MC2	103	8
MC3	324	20

Apparent activation energies for boehmite-based monocarbonates were also determined and results are listed in Table 7.

3. 3. IR Spectroscopy

The infrared spectrum of monocarbonate-containing product is shown in Figure 9. The spectrum shows only bands that can be attributed to the presence of monocarbonate[33, 35], hydrogarnet[34], portlandite[34], and calcite.[50, 51] Low-wavenumber bands (400–950 cm^{-1}) are indicative of Al–O groups originating from mainly isolated AlO_6 octahedra; bands in the range from 1000 to 1700 cm^{-1} represent CO_3^{2-} and H_2O vibrations, while the bands from 3000 to 3700 cm^{-1} show the presence of free and/or variously bonded OH^- groups.

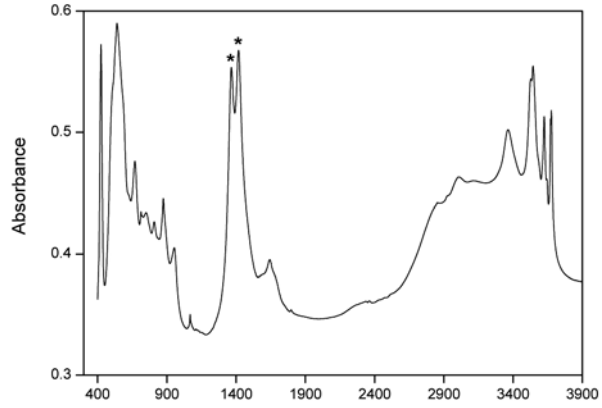

Figure 9. IR spectrum of a synthetic boehmite+calcite 4.2)-based monocarbonate*: monocarbonate CO_3^{2-} band splitting

Figure 9 also shows a $_3$ CO_3^{2-} band splitting into two bands that are a confirmatory evidence for the presence of monocarbonate.

The effects of different synthesis times and limestone sources used were not very distinct. There were only variations in absorbance values, mostly in monocarbonate-related CO_3^{2-} bands, that could be a consequence of different crystallinities of the products. Table 8 shows main IR band positions and their assignments.

Table 8. IR wavebands positions and their assignments for the spectrum shown in Figure 9.

Band (cm^{-1})	Assignment[(1)]	Band (cm^{-1})	Assignment[(2)]
424	AlO_6	405	AlO_6; C_3AH_6
539	AlO_6	713	CO_3^{2-}; $CaCO_3$
668	AlO_6	809	AlO_6; C_3AH_6
954	AlO_6	874	CO_3^{2-}; $CaCO_3$
1067	CO_3^{2-}	1643	H_2O
1365	CO_3^{2-}	3644	OH^-; $Ca(OH)_2$
1417	CO_3^{2-}	3668	OH^-, isolated
1645/1636 (sh)	H_2O		
3363	H_2O		
3543	H_2O		
3624	OH^-, associated		
3676	OH^-, free		

[(1)] Assigned to monocarbonate [(2)] Assigned to other constituents

3. 4. SEM

Figures 10 and 13 show SEM pictures of synthetic monocarbonates.

Monocarbonate crystals with hexagonal-like morphology were larger for gibbsite-based products irrespective of a limestone fraction used.

Figure 10. SEM picture of a boehmite-based monocarbonate (24 h; with calcite 4.2).

Figure 11. Detail of SEM picture of a boehmite-based monocarbonate from Fig. 7.

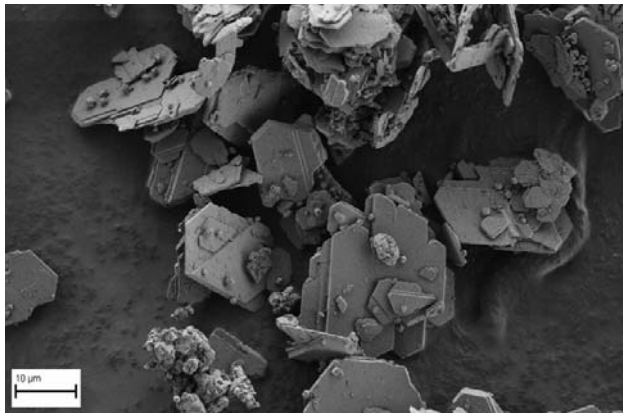

Figure 12. SEM picture of a gibbsite-based monocarbonate (24 h; calcite 4.2).

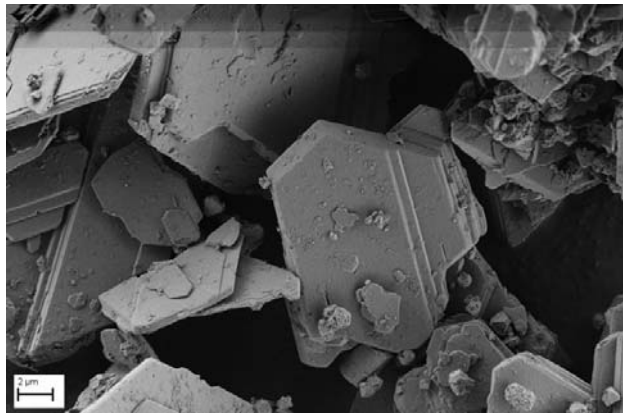

Figure 13. Detail of SEM picture of a gibbsite-based monocarbonate from Fig. 9.

4. Conclusion

The synthesis of monocarbonate was carried out from gibbsite, boehmite, portlandite and limestone at 80 °C with the synthesis times of 24 and 48 hours. Powder X-ray diffraction showed that monocarbonate, $C_4A\bar{C}H_{11}$, was the main reaction product along with a few reflections of limestone in certain products. Hydrogarnet, C_3AH_6, was also present in gibbsite-based monocarbonates. Crystallographic cell parameters were determined and they closely matched published data for a single crystal of monocarbonate that formed naturally over years within a concrete block.

The dehydration of gibbsite-based $C_4A\bar{C}H_{11}$ in the temperature range from 120 to 262 °C is a four-step process comprising two doublets. The water contents from the first dehydration doublet, MC1-MC2, decrease with longer synthesis time, whereas the opposite trend is evident for MC3 dehydration step. Only water contents of MC4 step show a dependency on the limestone fraction used; this unexpected behavior is currently being investigated.

The dehydration of boehmite-based $C_4A\bar{C}H_{11}$ is, in contrast to the above, only a three-step process comprising one doublet and one asymmetric peak. The influence of either limestone source or synthesis time on shapes of DTG curves and on their temperature maxima is insignificant. An increase in water contents of MC3 step is evident only when coarser fraction of limestone, calcite 4.2, is used.

Water from first dehydration doublet is weakly bound in gibbsite- and boehmite-based monocarbonates: a 2-hour heating at 110, 120 and 130 °C considerably decreases also the area of the second DTG peak at 153±2 °C. The activation energies for MC1 and MC2 dehydration steps are equal for gibbsite- and boehmite-based mono-

carbonates, 85 and 104 kJ/mole, respectively. Water content of the MC3 dehydration step exhibits higher activation energy for gibbsite-based monocarbonate (454 kJ/mole) than for boehmite-based one (324 kJ/mole).

Two-step dehydration of portlandite in all boehmite-based monocarbonates indicates in its first step the presence of finely dispersed microcrystalline portlandite that could only have formed topotactically through the decomposition-disproportionate reaction of C_3AH_6 at about 335 °C. The DTG temperature maxima of this form of portlandite appear at 395±1 °C. The areas under these DTG peaks increased significantly for 48-hour syntheses when coarser fraction of limestone, calcite 4.2, was used.

Contents of unreacted portlandite and limestone are lower in boehmite-based products than in gibbsite-based ones. Any individual content, determined by the thermogravimetric analysis, is between 1.8 and 3.5% and these materials must be of micron-size and finely dispersed within the product or even semicrystalline because X-ray diffraction did not always detect them. Thermogravimetric analysis and IR spectroscopy, however, clearly showed their presence.

The morphology of monocarbonates was that of a hexagonal-like platy crystals the dimension of which was distinctly larger for gibbsite-based products.

The formation of monocarbonate at 80 °C is conditioned by a combination of alumina- and calcite sources used. There is some indication that limestone particle size influences the water content of monocarbonate but additional work is currently being carried out in order to confirm this so far inconclusive evidence. An open question remains a high value of activation energy for the third step of monocarbonate dehydration.

Direct comparison between the synthetic monocarbonate and the one formed in hydrated cement-limestone system is, unfortunately, not possible, due to a small content of monocarbonate within the cement matrix. We have so far only established the evidence of a relation between fineness of limestone and the appearance of the high-temperature decarboxylation effect of monocarbonate in hydrated cement-limestone system.

5. Acknowledgments

The authors thank the Slovenian Research Agency for funding this research project (Grant P1-0021).

The authors also thank Magnesia GmbH, D-21311 Lüneburg, Germany, and Calcit d.o.o., SI-1242 Stahovica, Slovenia for donating calcite samples for this study.

The authors thank referees for their comments and suggestions.

6. References

1. W. Dosch, H. zur Strassen, Zem.-Kalk-Gips **1965**, *18*, 233–237.
2. M. T: Gaztanaga, S. Goni, A. Guerrero, in: R. J. Mangabhai, F. P. Glasser (Eds.), Calcium Aluminate Cements 2001, IOM Communications Ltd., London, **2001**, pp. 349–359.
3. E. Spohn, W. Lieber, Zem.-Kalk-Gips **1965**, *18*, 483–485
4. P. Fierens, A. Verhaegen, J. P. Verhaegen, Cem. Concr. Res. **1974**, *4*, 695–707.
5. J. Grandet, J. P. Ollivier, Cem. Concr. Res. **1980**, *10*, 759–770.
6. J.-P. Ollivier, J. Grandet, B. Thenoz, Bull. Minéral. **1982**, *105*, 267–272.
7. P. J. M. Monteiro, P. K. Mehta, Cem. Concr. Res. **1986**, *16*, 127–134.
8. V. L. Bonavetti, V. F. Rahhal, E. F. Irassar, Cem. Concr. Res. **2001**, *31*, 853–859.
9. B. Lothenbach, G. Le Saout, E. Gallucci, K. Scrivener, Cem. Concr. Res. **2008**, doi: 10. 1016/j. cemconres. 2008. 01. 002
10. K. Ingram, M. Poslusny, K. Daugherty, W. Rowe, in: P. Klieger, R. D. Hooton (Eds.): Carbonate Additions to Cement, STP 1064, ASTM, Philadelphia, **1990**, pp. 14–22.
11. K. D. Ingram, K. E. Daugherty, Cem. Concr. Comp. **1991**, *13*, 165–170.
12. W. Schwarz, in: W. Schwarz, K. Sujata, H. M. Jennings, A. Gerdes, H. Sadouki, F. H. Wittmann (Eds.): Chemically Modified Hydration of Portland Cement, Aedificatio Publishers, Freiburg i. Br., **1994**, pp. 5–47.
13. J. Péra, S. Husson, B. Guilhot, Cem. Concr. Comp. **1999**, *21*, 99–105.
14. G. Kakali, S. Tsivilis, E. Aggeli, M. Bati, Cem. Concr. Res. **2000**, *30*, 1073–1077.
15. P. Hawkins, P. D. Tennis, R. J. Detwiler, The Use of Limestone in Portland Cement: A State-of-the-Art Review, EB227, Portland Cement Association, Skokie, **2003**, 44 p.
16. D. P. Bentz, Cem. Concr. Comp. **2006**, *28*, 124–129.
17. R. Turriziani, G. Schippa, Ric. Sci. **1956**, *26*, 2792–2797.
18. E. T. Carlson, H. A. Berman, J. Res. N. B. S. **1960**, *64A*, 333–341.
19. P. L'Hopitallier, in: R. L. Blaine (Ed.): Chemistry of Cement, Proceedings of the 4th International Symposium, Washington 1960, Vol. II, National Bureau of Standards, Washington, **1960**, pp. 1007–1033.
20. P. Seligmann, N. R. Greening, Highway Res. Rec. **1964**, *No. 62*, 80–105.
21. H. F. W. Taylor, Cement Chemistry, Academic Press Ltd., London, **1990**, pp. 169–173.
22. W. A. Klemm, L. D. Adams, in: P. Klieger, R. D. Hooton (Eds.): Carbonate Additions to Cement, STP 1064, ASTM, Philadelphia, **1990**, pp. 60–72.
23. C. Andrade, J. L. Sagrera, A. Hidalgo, C. Alonso, in: R. J. Mangabhai, F. P. Glasser (Eds.): Calcium Aluminate Cements 2001, IOM Communications Ltd., London, **2001**, pp. 361–369.
24. M. A. Caldarone, Effect of Use of Limestone on Various Properties of Portland Cement, R&D Serial No. 2891, Portland Cement Association, Skokie**, 2006**, 13 p.

25. V. M. Sizyakov, V. O. Zakharzhevskaya, O. A. Borzenko, Russ. J. Appl. Chem. **1998**, *71*, 1470–1472.
26. V. M. Sizyakov, Russ. J. Appl. Chem. **1998**, *71*, 1473–1475.
27. D. L. Kantro, L. E. Copeland, E. R. Anderson, An X-ray diffraction investigation of hydrated portland cement paste, in: Proceedings of the ASTM, Vol. 60, ASTM, Philadelphia, **1960**, pp. 1020–1035.
28. Guide to Compounds of Interest in Cement and Concrete Research, Spec. Rep. 127, Highway Research Board, Washington D. C., **1972**, 53 p.
29. K. Mather, Transp. Res. Circ. **1976**, *No. 176*, 9–30.
30. R. L. Sharma, S. P. Pandey, Cem. Concr. Res. **1999**, *29*, 1525–1529.
31. N. A. Voglis, G. T. Kakali, S. G. Tsivilis, Mikrochim. Acta **2001**, *136*, 181–183.
32. J. Bensted, World Cem. Technol. **1980**, *11*, 395–406.
33. J. Bensted, World Cem. **1983**, *14*, 383–392.
34. J. Bensted, Applications of infrared spectroscopy to cement hydration, The Society of Chemical Industry Construction Materials Group and Institute of Materials Meeting on Techniques for Characterization of Cement Hydration, April 21, 1994, Society of Chemical Industry, London, **1994**, 55 p.
35. M. A. Trezza, A. E. Lavat, Cem. Concr. Res. **2001**, *31*, 869–872.
36. S. N. Ghosh, in:S. N. Ghosh (Ed.), Advances in Cement Technology: Chemistry, Manufacture and Testing, Tech Books Int., New Delhi, **2002**, pp. 709–734.
37. R. Fischer, H.-J. Kuzel, Cem. Concr. Res. **1982**, *12*, 517–526.
38. M. François, G. Renaudin, O. Evrard, Acta Cryst. **1998**, *C54*, 1214–1217.
39. G. Renaudin, M. François, O. Evrard, Cem. Concr. Res. **1999**, *29*, 63–69.
40. V. S. Ramachandran, Thermochim. Acta **1988**, *127*, 385–394.
41. S. Tsivilis, G. Kakali, E. Chaniotakis, A. Souvaridou, J. Therm. Anal. **1998**, *52*, 863–870.
42. J. Dweck, P. M. Buchler, A. C. V. Coelho, F. K. Cartledge, Thermochim. Acta **2000**, *346*, 105–113.
43. V. S. Ramachandran, R. M. Paroli, J. J. Beaudoin, A. H. Delgado, Handbook of Thermal Analysis of Construction Materials, William Andrew Publishing, Norwich, **2003**, 680 p.
44. J. I. Bhatty, F. M. Miller, in: J. I. Bhatty, F. M. Miller, S. H. Kosmatka (Eds.): Innovations in Portland Cement Manufacturing, Portland Cement Association, Skokie, **2004**, pp. 1037–1068.
45. T. J. B. Holland, S. A. T. Redfern, Miner. Mag. **1997**, *61*, 65–77.
46. V. S. Ramachandran, R. M. Paroli, J. J. Beaudoin, A. H. Delgado, Handbook of Thermal Analysis of Construction Materials, Noyes Publications, Norwich, **2002**, pp. 71–142.
47. V. S. Ramachandran, in: V. S. Ramachandran, J. J. Beaudoin (Eds.): Handbook of Analytical Techniques in Concrete Science and Technology, William Andrew Publishing/Noyes Publications, Norwich, **2001**, pp. 127–173.
48. T. Hatakeyama, Z. Liu (Eds.): Handbook of Thermal Analysis, John Wiley & Sons, Chichester, **1998**, p. 48.
49. H.-J. Kuzel, Neues Jahrb. Mineral. Monatsh. **1969**, 397–404.
50. W. B. White, in V. C. Farmer (Ed.): The Infrared Spectra of Minerals, Miner. Soc. Monograph 4, Mineralogical Society, London, **1974**, pp. 227–284.
51. F. A. Miller, in: D. W. Mayo, F. A. Miller, R. W. Hannah (Eds.): Course Notes on the Interpretation of Infrared and Raman Spectra, John Wiley & Sons, Inc., Hoboken, **2003**, pp. 297–354.

Povzetek

Kalcijev monokarboaluminat smo sintetizirali iz zmesi bemita ali gibsita ter apnenca in kalcijevega hidroksida pri 80 C v času 24 ur. Produkte smo okarakterizirali s praškovno rentgensko difrakcijo, termogravimetrično analizo, infrardečo spektroskopijo in vrstično elektronsko mikroskopijo. Produkti so se razlikovali po vsebnostih kalcijevega monokarboaluminata ter nezreagiranega apnenca ter kalcijevega hidroksida. Rentgensko difrakcijski posnetki ter infrardeči spektri sintetičnih kalcijevih monokarboaluminatov niso pokazali velikih razlik med različnimi produkti. Dimenzije heksagonalnih ploščatih kristalov kalcijevega monokarboaluminata so bile večje pri produktih, sintetiziranih iz gibsita. Dehidratacija kalcijevega monokarboaluminata je potekala v treh- ali štirih stopnjah v odvisnosti od kombinacije izhodnih surovin. Vpliv sinteznih pogojev na način dehidratacije je bil manj izrazit. Glavni vpliv na nastanek kalcijevega monokarboaluminata je imela kombinacija aluminijeve komponente ter dimenzije delcev apnenca.